Heat Transfer Engineering

Analysis of an Ultrathin Graphite-Based Compact Heat Exchanger

Alex Heltzel [a] , Columbia Mishra [b] , Rodney S. Ruoff [b c] & Andrew Fleming [d]

[a] PC Krause and Associates, Inc., West Lafayette, Indiana, USA

[b] Department of Mechanical Engineering, University of Texas at Austin, Austin, Texas, USA

[c] Texas Materials Institute, University of Texas at Austin, Austin, Texas, USA

[d] U.S. Air Force Research Laboratory, Wright-Patterson Air Force Base, Ohio, USA

PLEASE SCROLL DOWN FOR ARTICLE

Analysis of an Ultrathin Graphite-Based Compact Heat Exchanger

ALEX HELTZEL,[1] COLUMBIA MISHRA,[2] RODNEY S. RUOFF,[2,3]
and ANDREW FLEMING[4]

[1]PC Krause and Associates, Inc., West Lafayette, Indiana, USA
[2]Department of Mechanical Engineering, University of Texas at Austin, Austin, Texas, USA
[3]Texas Materials Institute, University of Texas at Austin, Austin, Texas, USA
[4]U.S. Air Force Research Laboratory, Wright–Patterson Air Force Base, Ohio, USA

The emerging production of ultrathin graphite material is applied to thermal management in a numerical comparison of aluminum and graphite-based plate-fin heat exchangers. Considering anisotropic thermal conductivity in which out-of-plane transport is about two orders of magnitude lower than in-plane values, the ultrathin graphite-based solution outperforms aluminum by rejecting up to 20% more heat on a volumetric basis. Thermal and hydraulic performance is characterized for both solutions over a range of airflow rates in a notional water/air device. Laminar through fully turbulent regimes are considered. Steady and unsteady three-dimensional (3-D) conjugate simulations reveal a faster equilibration rate for the ultrathin graphite-based solution, minimizing thermal lag that must be accounted for in on-demand electronics cooling. Fin optimization studies predict equivalent conductance with graphite at one-tenth the thickness of aluminum. The combination of improved heat rejection, rapid response rate, and low material density make an ultrathin graphite-based solution uniquely suited to aerospace thermal management.

INTRODUCTION

Extraordinary transport properties observed in graphene—a carbon monolayer arranged in a two-dimensional (2-D) honeycomb lattice—encourage its use in devices where conductive thermal diffusion is a limiting factor. Recent measurements by Cai et al. [1] report thermal conductivity, *k,* of supported graphene grown by chemical vapor deposition (CVD) as 2500 +1100/–1050 W/m-K at 250 K, and 1400 +500/–480 W/m-K near 500 K. Others have reported even higher in-plane values approaching 5000 W/m-K using an optical measurement technique on suspended large-area graphene flakes produced from standard mechanical exfoliation [2, 3]. Seol et al. [4] measured thermal conductivity of suspended graphene monolayers and

reported values in the range 3000–5000 W/m-K, exceeding the peak value of diamond. Molecular dynamics (MD) simulations [5] based on the Green–Kubo relations predict a room temperature thermal conductivity of 6000 W/m-K for an isolated graphene monolayer, and a value for *k* reduced by as much as a factor of 10 for stacked graphite due to interlayer coupling. Jiang et al. [6] calculated the thermal conductance of graphene in the pure ballistic limit, which translates to a thermal conductivity in excess of ∼6600 W/m-K. A calculation based on the Boltzmann equation predicts a peculiar dependence of *k* on the width of graphene nanoribbons and on the roughness of the edges, when the diffusive conduction dominates [7]. Recently, Guo et al. [8] used nonequilibrium molecular dynamics to investigate the conductivity of graphene nanoribbons with different edge shapes as a function of length, width, and strain, finding strong dependence on boundary/interface characteristics. The experimental work of Seol et al. [4] verified this by observing graphene supported on a silicon dioxide substrate. Phonon leakage and interface scattering reduced the suspended value given above to approximately 600 W/m-K, albeit still exceeding copper and aluminum by a wide margin. Boundary scattering

Address correspondence to Dr. Alex Heltzel, PC Krause and Associates, Inc., 3000 Kent Avenue, Suite C1-100, West Lafayette, IN 47906, USA. E-mail: heltzel@pcka.com

and weak out-of-plane bonds mean extreme anisotropy in the orthotropic conductivity of closely related three-dimensional (3-D) samples, such as highly oriented pyrolytic graphite (HOPG), from which graphene is often mechanically exfoliated. In-plane values of approximately 1600 W/m-K contrasting with out-of-plane values on the order of 10 W/m-K in the same sample have been reported [9]. Thermal conductivity of multilayer graphene has been found to be dependent on the number of atomic planes and approaches the bulk graphite limit of 2000 W/m-K [3, 10]. The variation in thermal conductivity with the number of atomic planes in multilayer graphene can be attributed to the strong coupling between the cross-plane phonon modes, which causes heat to propagate in all directions. Unlike in single-layer graphene, heat transport in basal planes of bulk graphite is 2-D only till some low-bound cutoff frequency. For single-layer graphene there are no transverse optical phonon branches that can contribute to the cross-plane heat transport at the long wavelength limit in the system. For multilayer graphene, on the other hand, the additional phonon branches increase the total number of phonon states available for three-phonon Umklapp scattering, and hence, low phonon group velocity, resulting in less effective heat transport and a lower value for thermal conductivity approaching that of bulk graphite. The present numerical work draws inspiration from the thermal transport of graphene, but considers multiple layers more appropriately referred to as ultrathin graphite. When considering graphene and ultrathin graphite-based composite materials for thermal application, conductive anisotropy must be noted carefully, including macroscopic orientation with respect to desired transport, and available techniques for minimizing resistance.

Bridging the gap from micro/nanoscale experimentation to device application requires technology to mass-fabricate macroscale foils of single- and multi-layer graphene as well as ultrathin graphite. Progress in pursuit of this goal has advanced rapidly since exfoliation of single-layer graphene in 2004, as a number of synthesis approaches have been reported. Mechanical exfoliation [11] was the first to isolate monolayers, but suffers from limited sample size and lack of scalability. It is possible to produce graphene oxide platelets in bulk through chemical reduction [12]; however, lattice imperfections during the reduction and film-production processes have, to date, led to degraded transport properties. Graphitization through annealing of a silicon carbide surface in an argon atmosphere produced micrometer-to-millimeter scale graphene domains with improved electron mobility, yet still low relative to that of graphite-derived graphene [13]. The approach of growing graphene on certain metals has also been successful [14, 15], though challenges regarding scaling size, effective transfer (graphene-on-insulator is desired for most applications), and expense remain. A corner may have been turned, however, with recent communications of large-area, high-quality graphene film generation. Postage-stamp-sized graphene films have been grown on copper foils by chemical vapor deposition, and transferred successfully to Si/SiO$_2$ wafers, while retaining excellent transport properties [16, 17]. Building from this work,

even larger 14-inch by 26-inch graphene sheets (30 inches along the diagonal) have been transferred to flexible target substrates, with the researchers reporting excellent electrical conductivity. The authors also provided a prototype of a touch-screen panel out of the material, connected to a personal computer (PC) with control software [18]. The pace of these developments highlights both the versatility of methods, and the high potential expected for graphene-based devices.

It is the authors' goal to accelerate the technology transfer process in the field of thermal management, an application area that has as yet been overshadowed by the exciting electrical properties of graphene. Thermal management potential has indeed been noted, however, particularly in the area of high-density heat dissipation in microelectronics packages [19].

Graphite as a heat spreader has great potential for high heat flux dissipation due to the ability of a graphite-based fin to entrain energy deeper into the coolant fluid volume. Noting the referenced manufacturing advances, this work intends to present and analyze a macroscale application with distinct suitability in the aerospace industry: an ultrathin graphite-based compact, plate-fin heat exchanger. The Air Force Research Laboratory has identified the need for characterization and scaling of emerging heat exchanger technologies. An accurate and efficient methodology will reduce expensive, time-consuming trial-and-error fabrication, as well as identify integration effects. In order to accomplish this, a fairly comprehensive modeling effort has been initiated which builds from work performed at several university, government, and industrial laboratories. Much of this work has focused on emerging microscale designs which seek to take advantage of inherent thermal rewards. The heat transfer advantage of microstructured flow passages has long been recognized. Tuckerman and Pease [20] conducted one of the early experimental studies, showing enhanced volumetric heat transfer in microchannel devices, due in part to large surface-area-to-volume ratios. Since then, this work has been confirmed and extended by various researchers using many different flow geometries. Liquid cooling in rectangular microchannels has demonstrated very high heat transfer rates in studies by Lee et al. [21] and Harris et al. [22], among others. Heat transfer and fluid dynamics modeling of such systems (at a very local level) has been presented by Li et al. [23], Fedorov and Viskanta [24], and Lee and Garimella [25], to name a few. In all cases, very high heat transfer rates were observed (0.1–1.0 kW/cm^2), due in part to substantial surface area, but also thinning of the hydrodynamic and thermal boundary layers. These heat transfer advantages are not surprising and conform with well-understood fundamentals of heat transfer. It was generally concluded that despite the small scale, the Navier–Stokes continuum treatment still applies and can accurately predict performance. Advances in manufacturing techniques and skillful engineering at the microscale, however, have led to testing and application only recently.

Despite the many advantages noted in the referenced works, microstructured heat exchangers are not unequivocally superior to macrostructured devices. The potential for large hydraulic

losses exist, and is discussed in more detail in the results section of this work. In an advanced aerospace platform, particularly tactical fighters, a pressure drop penalty in an airstream can be a notable concern. Smaller flow passages are also more susceptible to particulate clogging. Perry and Kandlikar [26] recognized the disadvantage in a study aimed at mitigating this potential drawback. While they found that high shear stresses prevent particulate clogging in the actual microchannels, the header regions can exhibit buildup. Fouling due to fibrous elements, on the other hand, was found to be very detrimental to pressure drop in the microchannels [26]. Another noteworthy consideration is the structural integrity of the system, particularly if there exists a large pressure differential between fluid streams in a heat exchanger with wall thicknesses as low as 40–50 μm. Both conventional stress deformation and electrostatic bonding can pose challenges, as observed by an industrial microchannel heat exchanger program [27]. The very high observed heat rates have also naturally led to proposed applications as evaporators, where the additional latent heat of a fluid can be accessed for cooling [28, 29]. In an aerospace platform, however, the added complexity of an evaporator/condenser apparatus could be burdensome in an already extraordinarily complex system. In addition, the orientation sensitivity of a two-phase system could become an issue in a vehicle with dynamic acceleration and gravity vectors (with respect to the device).

Compact heat exchanger fins fabricated from ultrathin graphite-based material have the potential to boost heat transfer without suffering a corresponding pressure drop or increased fouling risk. This material science development could dramatically affect the flux versus loss trade-off, with design implications at both the component level and thermal management system level in an integrated aerospace platform. Four heat exchangers are modeled here to provide quantitative insight into the emerging technology. Compact plate-fin designs utilizing both conventional aluminum and ultrathin graphite-based material with twenty fins per inch in water and air domains are directly simulated using 3-D solutions to the coupled Navier–Stokes and energy equations. Simulations are repeated for designs with thirty fins per inch, corresponding to flow passages of roughly 850 μm. Comparisons reveal the distinct dependence on fin conduction properties in-plane, along with the relative independence on out-of-plane conduction.

MODEL DEVELOPMENT

The challenge of modeling a macroscale heat exchanger core consisting of many thousands of microscale flow passages (and intermediate solids) is reduced by considering a small portion of the core. Symmetry in the no-flow direction is used, and the simulation domain can be recycled with boundary-condition mapping to simulate arbitrary size in the two flow directions. Fluid dynamics are modeled in both hot and cold fluids, and heat transfer is modeled in both hot and cold fluid streams as well as
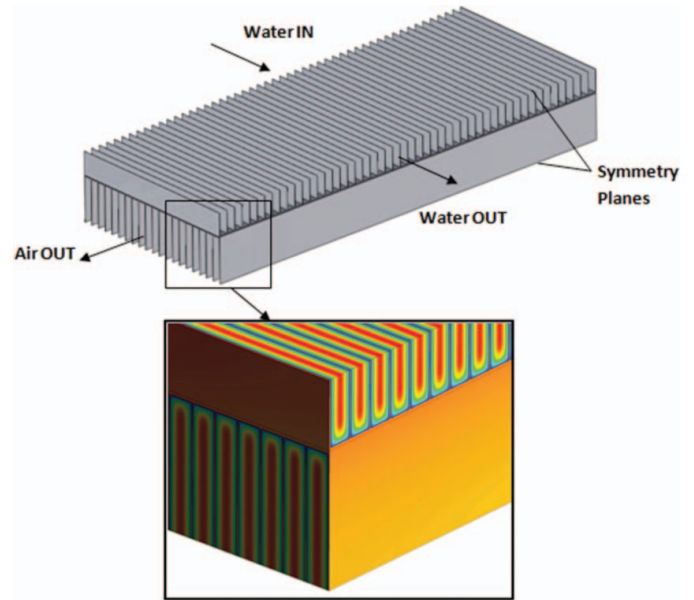

Figure 1 Compact plate-fin heat exchanger segment simulated using 3-D conjugate fluid dynamics and heat transfer. Predicted velocity and temperature profile. (Color figure available online.)

the intermediate solid. For the purposes of this demonstration work, a small section of a cross-flow plate-fin heat exchanger is modeled as pictured in Figure 1. The commercial computational fluid dynamics (CFD) solver ANSYS CFX 12.0 [30] is used to solve the Navier–Stokes and energy equations within the three-dimensional geometries. Solutions were verified with the FLUENT package [31]. The unsteady continuity, momentum, and total energy equations solved are given by

$$\frac{\partial \rho}{\partial t} + \nabla(\rho \vec{V}) = 0 \tag{1}$$

$$\frac{\partial \rho \vec{V}}{\partial t} + \vec{V} \cdot \nabla(\rho \vec{V}) = -\nabla P + \nabla \cdot \tau \tag{2}$$

$$\frac{\partial(\rho h_{tot})}{\partial t} - \frac{\partial \rho}{\partial t} + \nabla \cdot (\rho \vec{V} h_{tot}) = \nabla \cdot (k \nabla T)$$
$$+ \nabla \cdot (\vec{V} \cdot \tau) \tag{3}$$

where τ is the stress tensor, and the total enthalpy h_{tot} is related to the static enthalpy by

$$h_{tot} = h_s + \frac{1}{2} \vec{V}^2 \tag{4}$$

In Eqs. (1)–(4), ρ represents fluid density, P is pressure, $\vec{V}$ is the velocity vector, T is temperature, k is thermal conductivity, and t is time. Steady-state simulations are performed by implicitly solving the equations with the time-varying terms set to zero. Both unsteady and steady-state simulations were conducted during this effort.

The heat exchanger segments presented in this work simulate heat transfer between liquid water and air. In this situation, the air-side convective thermal resistance would dominate all thermal resistances. It is most appropriate to isolate air-side performance, then, by holding water-side properties constant over a range of simulations. Water is modeled entering the heat exchanger segment at a relatively low flow rate of 0.2 m/s and temperature of 370 K. This is considered laminar flow in all cases. Air is modeled entering the heat exchanger at flow rates between 1.0 and 30.0 m/s at 300 K, and therefore represents the cold side. The magnitude of temperatures considered does not require radiation models. Turbulence models are used when flow conditions imply their significance. In addition to the laminar flow assumption at the lowest air flow rates, the k-ε turbulence model is used at varying intensities (1%, 5%, and 10%) at Reynolds number >2300. Water is modeled as an incompressible fluid with viscous thermal dissipation, and air is modeled as an ideal gas. Redlich–Kwong and Vukalovich virial equations of state are also available for simulating real gases. Thermal conductivity for aluminum is temperature dependent and isotropic (237.0 W/m-K at 300 K). Thermal conductivity for ultrathin graphite is defined as 1580 W/m-K in-plane (aligned with the plane of the fins for each side of the heat exchanger) and 8.0 W/m-K out-of-plane. These values are based on the early work of Taylor [9], who characterized thermal transport in HOPG.

Numerical meshes were built and tested in ANSYS Workbench. Mesoscale flow simulations typically require finer mesh resolution due to the dominant influence of boundary-layer growth relative to a macroscale geometry with proportional, scaled-up dimensions. Resolution of approximately 10 μm is preferred in these regions, while sizing functions allowed element growth to 100 μm away from the solid/liquid interfaces. Referring to Figure 1, the unit simulation cell consists of 10 air channels aligned perpendicularly to 25 water channels, with fluid volumes separated by a 300-μm aluminum sheet. Channel widths are varied in this study from 850 μm to 1.27 mm (representing fin densities of 20/inch to 30/inch); 75-μm-thickness aluminum fins are simulated. Water channel depth is defined to be 6.35 mm, with air channel depth defined to be 12.7 mm. Symmetry allows each fluid channel height to be sliced in half, with symmetry planes modeled at these boundaries. Discretization required roughly 2 million nodes, with models of 10 million nodes tested for grid independence. Simulation domains were decomposed for local parallel processing using MPI protocols. Steady-state simulations conducted on a four-processor, 3.2-Ghz Intel machine required between 1 and 10 h, depending on geometry, Reynolds number, and turbulence model employed. Unsteady simulations using four processors required between 48 and 96 h per run.

RESULTS AND ANALYSIS

Though the focus of this work is ultrathin graphite-based heat exchanger core performance, several simulations corresponding
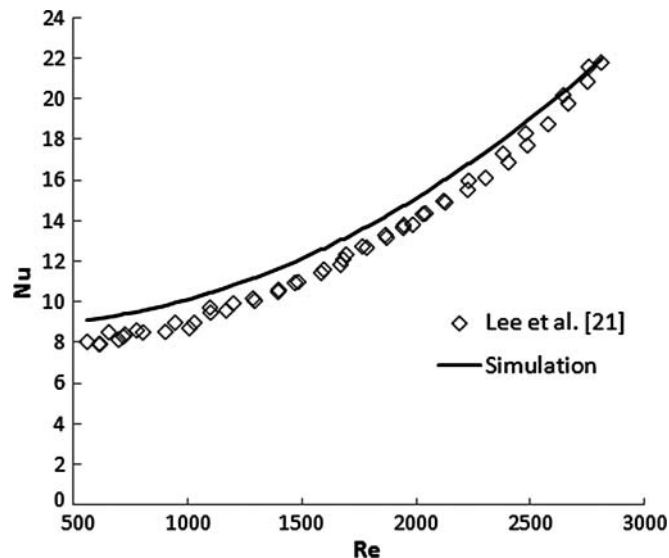

Figure 2 Predicted and observed [21] Nusselt number in 194 μm × 884 μm × 25.4 mm microchannel as a function of Reynolds number.

to experimental work on similar geometries were conducted for the purpose of verification and validation. A single study is presented here. Figures 2 and 3 compare predictions to the measured data of Lee et al. [21] obtained from Purdue University's Cooling Research Center, where microchannels were fabricated in copper. The observed Reynolds number, $Re = \rho V D / \mu$, where D is hydraulic diameter and μ is dynamic viscosity, passes from laminar through transitional and into turbulent flow for both cases. Medium intensity turbulence (5%) was simulated using the k-ε model above $Re = 1500$. The simulations accurately predict heat transfer performance in terms of Nusselt number, $Nu = h D / k$, including the gradual change in derivative characteristic of transition to turbulent flow. Hydraulic loss predictions in
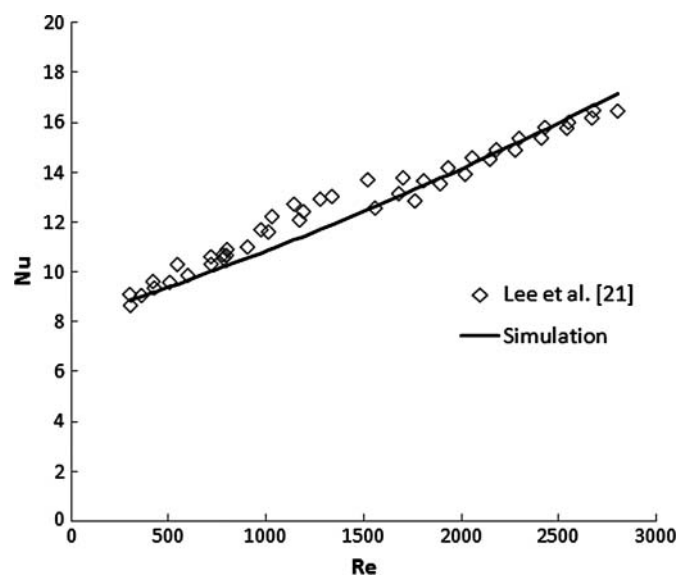

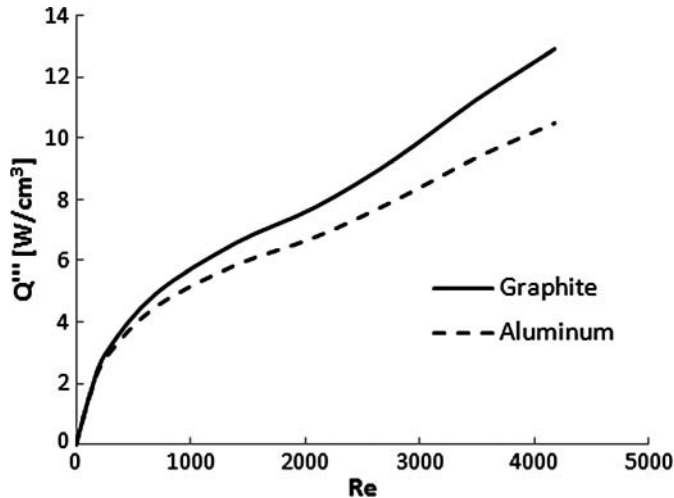**Figure 3** Predicted and observed [21] Nusselt number in 534 μm × 2910 μm × 25.4 mm microchannel as a function of Reynolds number.

Figure 4 Volumetric heat flux rejected by aluminum and ultrathin graphite-based heat exchanger segments, 20 fins/inch, $\Delta T = 70°C$.

microchannels were found to be similarly accurate [32]. Based on a somewhat larger sampling of comparisons to academic and industrial experiment, confidence exists in the ability to model heat transfer and pressure drops in a variety of micro- and mesoscale systems similar to the plate-fin design.

Figures 4 and 5 present the volumetric heat transfer rates between hot water and air coolant generated by aluminum and ultrathin graphite-based designs as a function of Reynolds number, with an inlet temperature difference of 70°C. Calculated volumes contain both solid and fluid domains. Figure 4, which refers to the design utilizing 20 fins per inch, indicates a noticeable flux enhancement due to the use of ultrathin graphite material. This improvement is magnified at higher flow rates and continues to increase in the fully turbulent regime, where the slope of the flux curve increases. At the highest flow rate considered, equivalent to 30.0 m/s at the air inlets, the ultrathin graphite-based design rejects 22% more energy to the air

stream than the aluminum design. Figure 5 presents similar results for the case of 30 fins per inch. At 30.0 m/s the ultrathin graphite-based design rejects a nearly identical 23% more energy to the air stream than the aluminum design. Note that the increased surface area per unit volume for the 30 fins per inch case also dramatically increases the overall heat rejection. We anticipate the rejection values to converge with decreasing fin depths, rather than fin density, since the source of the ultrathin graphite advantage is increased conduction to the center of the flow passage. From a design perspective, this indicates that the greatest opportunity for thermal performance gain through ultrathin graphite occurs in situations where the pressure-loss budget is minimal. It should be noted that unknown interfacial resistances were not included in either model, though these mechanisms would typically be shared between designs and therefore not affect the qualitative aspect of the results.

The anisotropy of graphite plays an interesting role in the modeled design. In the fins, two orders of magnitude difference in conduction length exists in the fin length direction (high conductivity) compared to the fin thickness direction (low conductivity). The conjugate effect, which utilizes higher delta T values over the whole fin surface, therefore outweighs the effect of reduced transport from fin core to fin surface.

The trade-off between increased fin density and hydraulic loss is illustrated by comparing Figures 4 and 5 with Figure 6, which plots the air-side pressure drop as a function of flow rate for both geometries. It is clear the thermal performance improvement of higher fin density comes with great cost. Thirty fins per inch boosts heat rejection by up to 49% relative to 20 fins per-inch, but with an even greater 53% jump in maximum pressure drop. The slightly higher pressure drops induced by the ultrathin graphite-based designs are simply a function of more heat added to the airstream, a small-scale propulsion effect. The relationships between pressure drop, fin density, and flow rates are well known, but the possibility of using an ultrathin graphite-based material to mimic the performance benefits of additional

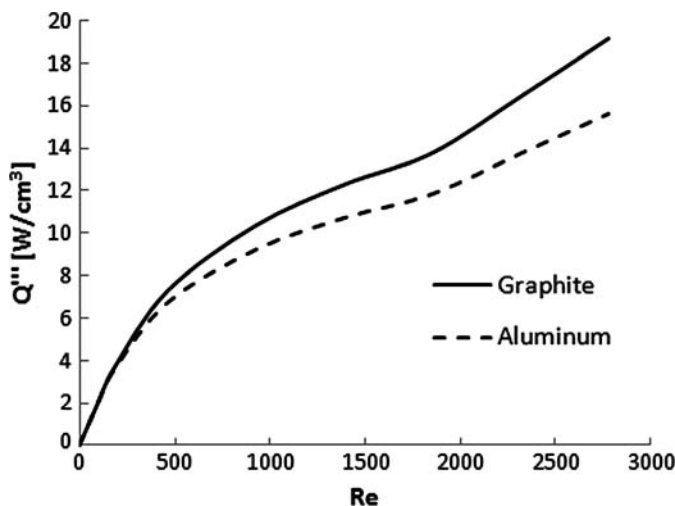**Figure 5** Volumetric heat flux rejected by aluminum and ultrathin graphite-based heat exchanger segments, 30 fins/inch, $\Delta T = 70°C$.
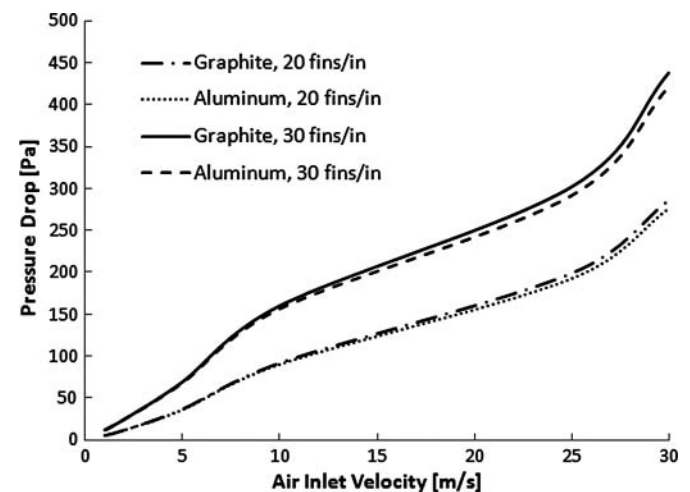

Figure 6 Pressure drop induced by ultrathin graphite and aluminum designs of two fin densities as a function of air inlet velocity.

fins without sacrificing the large corresponding loss is unique to the work presented in these figures. Material benefits extend even past the fluid/thermal considerations, as the density of 3-D HOPG is approximately 2.1–2.2 g/cm^3, while the value for aluminum is 2.7 g/cm^3. Whether or not the ultrathin graphite-based structural material retains this mass advantage is a function of the referenced emerging manufacturing techniques, even a 5–10% improvement would be notable. For tactical aerospace applications, a device manufactured with substantial weight savings in addition to these predicted performance benefits represents a technology enabler, in which the bottleneck of thermal systems management is opened.

The advantage of being able to predict transient characteristics of heat exchangers is twofold. At a component level, the thermal capacitance of a heat exchanger is a performance characteristic, often closely correlated with the mass of the device. Many land-based applications are not sensitive to thermal lag—the equilibration time of a heat exchanger to changes in environmental variables. Aerospace applications, however, often involve cooling of controllers, power electronics, and other sensitive equipment that can experience dynamic changes in waste heat generation and associated cooling requirements. If allowed to persist for even short periods of time, hot spots and exceeded temperature thresholds can cause permanent damage and potential system failure. Therefore, the temporal response of a cold fluid loop to changes in the hot fluid loop can be of considerable importance in some situations. Second, all major airframe manufacturers routinely build system-level models as a means of analyzing integrated performance. These dynamic models can rely on stepping between steady-state design points or true dynamic integration, but a critical role is the diagnosis of unintuitive issues resulting from the assembly of a complex system of components. This can include exceeding individual component thresholds for short periods of time. One advantage of the methodology presented here is the availability of response curves for implementation in these larger models. An accurate dynamic representation of the effect these heat exchanger have on the entire thermal subsystem can thus be modeled.

The two mechanisms of finite response time are fluid residence time and thermal capacitance of the solid. For the conditions modeled in this work, the capacitance effect dominates, as residence times are a small fraction of a second, roughly two orders of magnitude smaller than the predicted lags. Thermal lag on the cold side of the heat exchanger is accompanied by a heat-soak effect on the hot side, in which an abrupt change in flow rate or temperature temporarily thins a boundary layer and/or triggers a temporarily high temperature gradient between the fluid and solid. This would be most apparent in a device with a large amount of surface area or boundary-layer-thinning obstructions. Two fundamental transients are modeled in this work. With a steady-state solution found for the case of air inlet velocity equal to 5.0 m/s, air inlet temperature of 300 K, and water inlet conditions maintained at 0.2 m/s and 370 K, the air inlet velocity is perturbed to 15.0 m/s. This is referred to as the fluid perturbation. The second transient case models air inlet flow of
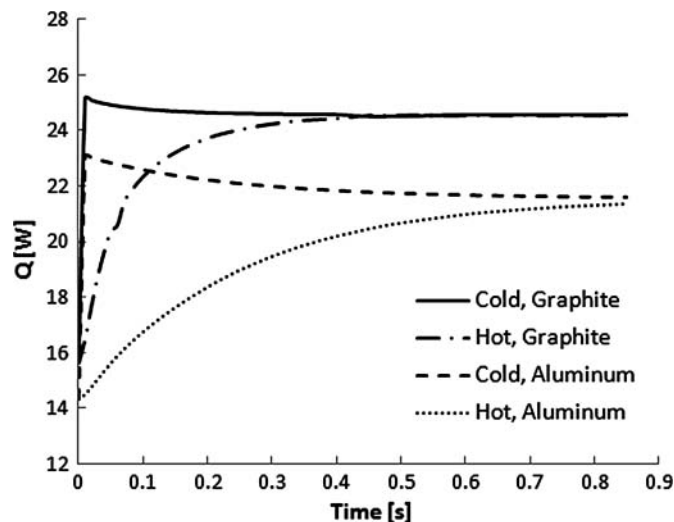

Figure 7 Transient response of aluminum and ultrathin graphite-based heat exchanger segments to an instantaneous flow perturbation.

10.0 m/s at 340 K and water inlet conditions maintained at 0.2 m/s and 370 K, with the air inlet condition perturbed to 300 K at time t = 0 s. This case is referred to as the thermal perturbation. Figure 7 plots the absolute flux as a function of time for identical fluid perturbations subjected to aluminum and ultrathin graphite-based heat exchangers. Figure 7 predicts a significantly faster response time for the ultrathin graphite-based device. If we define a metric wherein equilibration is reached when 95% of the change in flux is realized, then the ultrathin graphite-based heat exchanger achieves this equilibration in less than 50% of the time it takes for the aluminum heat exchanger to equilibrate. The total response times are on the order of 1 s, which can be ignored for most mechanical heating/cooling operations but may present challenges for sensitive electronics cooling that dissipate a large fraction of their input power as heat and operate on shorter-term cycles.

Figure 8 presents the equilibration times predicted as a result of the thermal perturbation to both devices. Again, the ultrathin graphite-based design reacts much faster to the step change in boundary condition, equilibrating in just 43% of the time of the aluminum design. With all flow conditions identical between designs in both perturbation schemes, Figures 7 and 8 predict larger fluxes after equilibration for the ultrathin graphite-based device, consistent with the steady-state investigations.

Fin thickness becomes an important design parameter where the use of multilayer graphene and ultrathin graphite requires advanced fabrication techniques. Reduced thickness is desirable from both manufacturing and HX core weight considerations. Based on the simple conductance relationship, ultrathin graphite would be expected to admit the same quantity of heat through an aluminum fin proportionately thicker than the materials' thermal conductivity values. For a 75-μm-thickness aluminum fin, equivalent conductance (in W/K) through ultrathin graphite could be expected at $75/(1580/237) = 11.25$ μm. The presence of a viscous, convective boundary, however, introduces
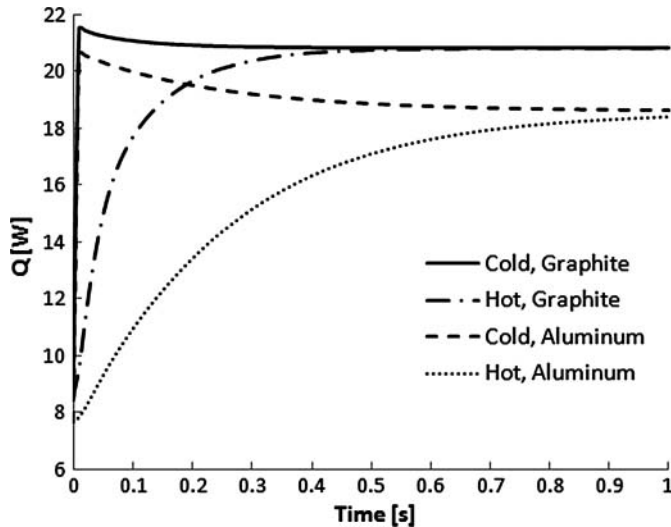
Figure 8 Transient response of aluminum and ultrathin graphite-based heat exchanger segments to an instantaneous thermal perturbation.

Figure 10 Normalized heat transfer by aluminum and ultrathin graphite-based heat exchanger segments, of 6.35 mm air channel height and varying fin thickness.

complexity that can be addressed only through a conjugate analysis. Simulations are performed for two separate fin heights of 6.35 mm and 12.7 mm. The working fluid modeled is turbulent air, entering the channel at 30.0 m/s. Figures 9 and 10 predict the heat transfer, normalized against the baseline of an aluminum fin of 75 μm thickness. With identical thicknesses at 12.7 mm channel height, greater than 20% more heat is transferred, replicating earlier results. Equivalent fin performance is predicted with graphite thickness of approximately 7 μm, or several micrometers thinner than what the basic conductance equation predicts, shown earlier. The curve indicates a steep conductance gain between 7 and 20 μm thickness, after which increasing thickness boosts conductance in a fairly shallow, linear manner.

Figure 10 illustrates the reduced benefit of high conductivity fins in channels of shorter height. Channels of height 6.35 mm
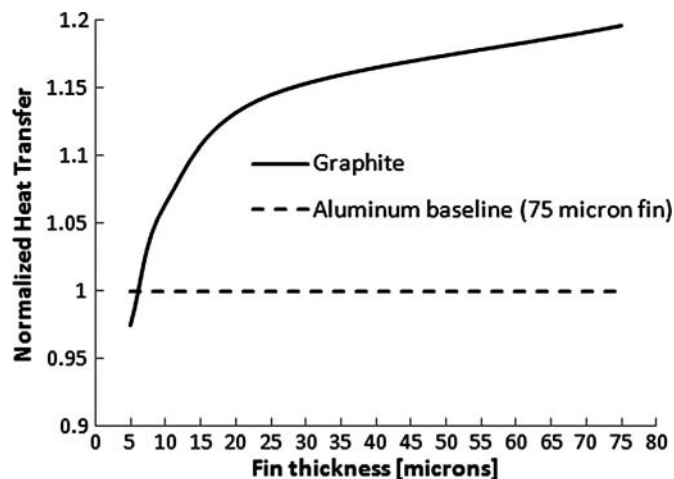
require only 3.175 mm of conduction length to the center of the channel, allowing aluminum to come within 6% of ultrathin graphite performance with identical fin thickness. This result supports the conclusion that the primary thermal advantage of ultrathin graphite is the ability to entrain energy more efficiently into the fluid volume by virtue of its higher thermal conductivity in this direction. The reduced fin height does not measurably affect the equivalent conductance thickness of ∼7 μm, nor the trend toward linearity after ∼25 μm.

A final study highlights the potential weight savings of an ultrathin-graphite-based heat exchanger. Figure 11 presents the results of the fin thickness simulations in terms of heat transfer per unit mass (per degree temperature difference). The baseline comparison value is that of an aluminum heat exchanger utilizing conventional 75-μm fins. Fin density is 20/inch for both designs. Mass density of highly oriented pyrolytic

Figure 9 Normalized heat transfer by aluminum and ultrathin graphite-based heat exchanger segments, of 12.7 mm air channel height and varying fin thickness.
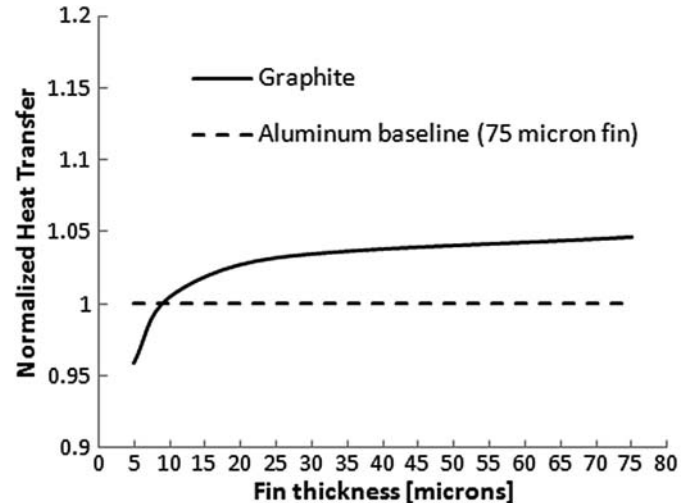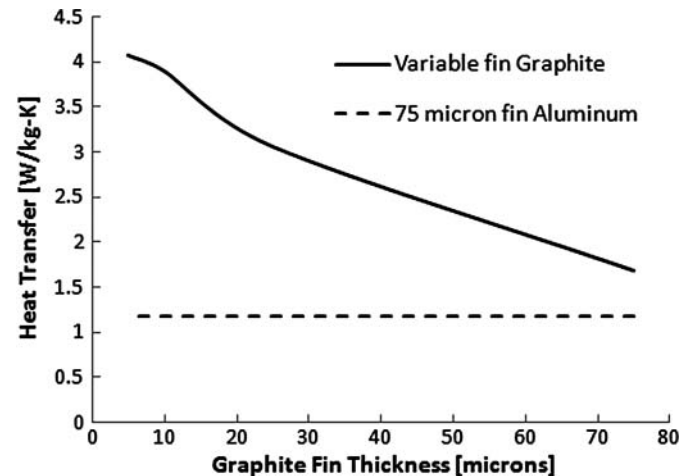

Figure 11 Heat transfer per unit mass, per degree temperature difference, in an ultrathin graphite-based heat exchanger segment compared to baseline aluminum with 75 μm fins.

graphite is taken to be 2270 kg/m^3, compared to 2700 kg/m^3 for aluminum. Heat transfer values at the far right of the plot in Figure 11, where graphite fins are of identical dimension to the aluminum, predict a modest reduction in total HX core weight for carbon. Values at the far left, where the thermal performances of the aluminum- and graphite-based heat exchangers are roughly equivalent, predict a more significant reduction in weight for the ultrathin graphite-based devices. This curve is based on a fully carbon-derived structure and would therefore be affected by metallic shell and supports necessary for manufacturing and installation integrity. In aerospace vehicles, heat exchangers represent considerable mass in the power and thermal management subsystem. The opportunity to provide performance consistent with current designs with nontrivial weight reduction would directly affect the system-level design envelope.

The challenge of manufacturing this type of 3-D structure from ultrathin graphite is nontrivial but surmountable, in the authors' opinions. Manifold, installation, and some structural components would necessarily remain metal. Bonding ultrathin graphite segments to metals in a thermally efficient manner is one of the challenges that begets the most attention. Despite the real manufacturing issues associated with fabricating a macroscale object from microscale elements, the pace of progress is such that optimism is justified. In particular, the weight savings demonstrated by the fin studies can be realized through bottom-up fabrication methods, extensions of those used to fabricate mono- and multilayer graphene.

CONCLUSIONS

Ultrathin graphite is proposed as a thermal management material due to its exceptional inherent transport properties. Recent studies have identified in-plane thermal conductivity in the 2-D carbon lattice exceeding that of all other known materials. While reduced in three dimensions, the anisotropic conductivity of ultrathin graphite is still superior to most common materials. Further, advances in manufacturing procedures are introducing both graphene and ultrathin graphite as an option in macroscale device application. The performance of a notional, ultrathin graphite-based plate-fin heat exchanger is tested through numerical comparison to a contemporary aluminum design. The graphite-based device outperforms aluminum, rejecting greater than 20% more energy to an air coolant stream at Reynolds numbers of 3000–4000. Unsteady simulations characterize the response time of the ultrathin graphite-based designs, predicting equilibration to fluid and thermal perturbations in approximately half the time of the aluminum device. Reducing the thickness of graphite fins reduces the total heat conduction, with fins of approximately 7.0 μm thickness performing equivalently to 75.0-μm aluminum fins. Given the anticipated manufacturing complexity of ultrathin graphite structures, curves are presented to trade performance advantage against fin thickness. The potential for increased volumetric efficiency generated by a lighter weight heat exchanger core has noteworthy system-level design consequences, particularly in the aerospace industry.

NOMENCLATURE

D   hydraulic diameter, m
h heat transfer coefficient, W m^{-2} K^{-1}
h_s static enthalpy, kg m^2 s^{-2}
h_{tot} total enthalpy, kg m^2 s^{-2}
k thermal conductivity, W m^{-1} K^{-1}
Nu   Nusselt number, Nu = h D/k
P pressure, Pa
Q   heat rate, W
Q'''   volumetric heat transfer, W cm^{-3}
Re   Reynolds number, Re = ρ V D/μ
t time, s
T temperature, K
$\vec{V}$ velocity vector, m s^{-1}

Greek Symbols

ρ   fluid density, kg m^{-3}
τ   stress tensor, Pa
μ   dynamic viscosity, kg m^{-1} s^{-1}

REFERENCES

[1] Cai, W., Moore, A. L., Zhu, Y., Li, X., Chen, S., Shi, L., and Ruoff, R. S., Thermal Transport in Suspended and Supported Monolayer Graphene Grown by Chemical Vapor Deposition, *Nano Letters*, vol. 10, pp. 1645–1651, 2010.

[2] Balandin, A. A., Ghosh, S., Bao, W. Z., Calizo, I., Teweldebrhan, D., Miao, F., and Lau, C. N., Superior Thermal Conductivity of Single-Layer Graphene, *Nano Letters*, vol. 8, no. 3, pp. 902–907, 2008.

[3] Ghosh, S., Bao, W., Nika, D. L., Subrina, S., Pokatilov, E. P., Lau, C. N., and Balandin, A.A., Dimensional Crossover of Thermal Transport in Few-Layer Graphene, *Nature Materials*, vol. 9, pp. 555–558, 2010.

[4] Seol, J. H., Jo, I., Moore, A. L., Lindsay, L., Aitken, Z. H., Pettes, M. T., Li, X. S., Yao, Z., Huang, R., Broido, D., Mingo, N., Ruoff, R. S., and Shi, L., Two-Dimensional Phonon Transport in Supported Graphene, *Science*, vol. 328, no. 5975, pp. 213–216, 2010.

[5] Berber, S., Kwon, Y. K., and Tomanek, D., Unusually High Thermal Conductivity of Carbon Nanotubes, *Physical Review Letters*, vol. 84, no. 20, pp. 4613–4616, 2000.

[6] Jiang, J. W., Wang, J. S., and Li, B., Thermal Conductance of Graphene and Dimerite, *Physical Review B*, vol. 79, 205418, 2009.

[7] Nika, D. L., Pokatilov, E. P., Askerov, A. S., and Balandin, A. A., Phonon Thermal Conduction in Graphene: Umklapp and Edge Roughness Scattering, *Physical Review B*, vol. 79, 155413, 2009.

[8] Guo, Z., Zhang, D., and Gong, X.-G., Thermal Conductivity of Graphene Nanoribbons, *Applied Physics Letters*, vol. 95, no. 16, 163103-3, 2009.

[9] Taylor, R., The Thermal Conductivity of Pyrolytic Graphite, *Philosophical Magazine*, vol. 13, no. 121, pp. 157–166, 1966.

[10] Nika, D. L., Ghosh, S., Pokatilov, E. P., and Balandin, A. A., Lattice Thermal Conductivity of Graphene Flakes: Comparison With Bulk Graphite, *Applied Physics Letters*, vol. 94, 203103, 2009.

[11] Novoselov, K. S., Geim, A. K., Morozov, S. V., Jiang, D., Zhang, Y., Dubonos, S. V., Grigorieva, I. V., and Firsov, A. A., Electric Field Effect in Atomically Thin Carbon Films, *Science*, vol. 306, no. 5696, pp. 666–669, 2004.

[12] Park, S., and Ruoff, R. S., Chemical Methods for the Production of Graphenes. *Nature Nanotechnology*, vol. 4, pp. 217–224, 2009.

[13] Emtsev, K. V., Bostwick, A., Horn, K., Jobst, J., Kellog, G.L., Ley, L., McChesney, J. L., Ohta, T., Reshanov, S. A., Rohrl, J., Rotenberg, E., Schmid, A. K., Waldmann, D., Weber, H. B., and Seyller, T., Towards Wafer-Size Graphene Layers by Atmospheric Pressure Graphitization of Silicon Carbide, *Nature Materials*, vol. 8, no. 3, pp. 203–207, 2009.

[14] Kim, K. S., Zhao, Y., Jang, H., Lee, S. Y., Kim, J. M., Ahn, J. H., Kim, P., Choi, J. Y., and Hong, B. H., Large-Scale Pattern Growth of Graphene Films for Stretchable Transparent Electrodes, *Nature*, vol. 457, pp. 706–710, 2009.

[15] Reina, A, Jia, X. T., Ho, J., Nezich, D., Son, H. B., Bulovic, V., Dresselhaus, M. S., and Kong, J., Large Area, Few-Layer Graphene Films on Arbitrary Substrates by Chemical Vapor Deposition, *Nano Letters*, vol. 9, pp. 30–35, 2009.

[16] Li, X., Zhu, Y., Cai, W., Borysiak, M., Han, B., Chen, D., Piner, R. D., Colombo, L., and Ruoff, R. S., Transfer of Large-Area Graphene Films for High-Performance Transparent Conductive Electrodes, *Nano Letters*, vol. 9, pp. 4359–4363, 2009.

[17] Li, X. S., Cai, W. W., An, J. H.; Kim, S., Nah, J., Yang, D. X., Piner, R. D., Velamakanni, A., Jung, I., Tutuc, E., Banerjee, S. K., Colombo, L., and Ruoff, R. S., Large-Area Synthesis of High-Quality and Uniform Graphene films on Copper Foils, *Science*, vol. 324, pp. 1312–1314, 2009.

[18] Bae, S., Kim, H., Lee, Y., Xu, X., Park, J., Zheng, Y., Balakrishnan, J., Im, D., Lei, T., Song, Y., Kim, Y., Kim, K., Ozyimaz, B., Ahn, J., Hong, B., and Iijima, S., 30-Inch Roll-Based Production of High-Quality Graphene Films

for Flexible Transparent Electrodes, *Nature Nanotechnology*, vol. 5, pp. 574–578, 2010.

[19] Ghosh, S., Calizo, I., Teweldebrhan, D., Pokatilov, E. P., Nika, D. L., Balandin, A. A., Bao, W., Miao, F., and Lau, C. N., Extremely High Thermal Conductivity of Graphene: Prospects for Thermal Management Applications in Nanoelectronic Circuits, *Applied Physics Letters*, vol. 92, 151911, 2008.

[20] Tuckerman, D. B., and Pease, R. F. W., High Performance Heat Sinking for VLSI, *IEEE Electron. Device. Lett.*, vol. EDL-2(5), pp. 126–129, 1981.

[21] Lee, P.-S., Garimella, S., and Liu, D., Investigation of Heat Transfer in Rectangular Microchannels, *International Journal of.\ Heat and Mass Transfer*, vol. 48, pp. 1688–1704, 2005.

[22] Harris, C., Kelly, K., Wang, T., McCandless, A., and Motakef, S., Fabrication, Modeling, and Testing, of Micro-Cross-Flow Heat Exchangers, *Journal of Microelectronic Systems*, vol. 11, pp. 726–735, 2002.

[23] Li, J., Peterson, G. P., and Cheng, P., Three-Dimensional Analysis of Heat Transfer in a Micro-Heat Sink With Single Phase Flow, *International Journal of Heat and Mass Transfer*, vol. 47, pp. 4215–4231, 2004.

[24] Fedorov, A. G., and Viskanta, R., Three Dimensional Conjugate Heat Transfer in the Microchannel Heat Sink for Electronic Cooling, *International Journal of Heat and Mass Transfer*, vol. 43, pp. 399–415, 2000.

[25] Lee, P.-S., and Garimella, S. V., Thermally Developing Flow and Heat Transfer in Rectangular Microchannels of Different Aspect Ratios, *International Journal of Heat and Mass Transfer*, vol. 49, pp. 3060–3067, 2006.

[26] Perry, J. L., and Kandlikar, S. G., Investigation of Fouling and Its Mitigation in Silicon Microchannels, *Proc. ICNMM2008*, Darmstadt, Germany, pp. 1–18, 2008.

[27] Williams, M., Bolla, J., Strumpf, H., and Muley, A., Advanced Heat Exchanger Technology for Aerospace Application, Proc. SAE Power Systems Conference, Seattle, WA, 2008-01-2903, 2008.

[28] Kandlikar, S. G., Heat Transfer Mechanisms During Flow Boiling in Microchannels, *Journal of Heat Transfer*, vol. 126, pp. 8–16, 2004.

[29] Liu, D., and Garimella, S., Flow Boiling Heat Transfer in Microchannels, *Journal of Heat Transfer*, vol. 129, pp. 1321–1332, 2007.

[30] ANSYS® CFX 12.1, User Manual, ANSYS, Inc.

[31] ANSYS® FLUENT, User Manual, ANSYS, Inc.

[32] Lelea, D., Nishio, S., and Takano, K., The Experimental Research on Microtube Heat Transfer and Fluid Flow of Distilled Water, *International Journal of Heat and Mass Transfer*, vol. 47, pp. 2817–2830, 2004.

Alex Heltzel is a senior engineer at PC Krause and Associates, Inc. (PCKA). He earned a Ph.D. in mechanical engineering (thermal/fluids systems) from the University of Texas at Austin in 2006. Prior to joining PCKA, he performed computational research at the Air Force Research Laboratory in support of low-temperature jet fuel stability. He has acted as a consultant to technology startup companies, and authored several book chapters and papers in the fields of micro-/nanoscale energy transport, near-field optics, and plasmonics.

Columbia Mishra is a Ph.D. student in the Department of Mechanical Engineering at the University of Texas at Austin, in the thermal/fluids systems track. She worked as an analyst at Stress Engineering Services, Inc., in Houston, TX, for a year after completing her M.S. in mechanical engineering at Texas Tech University in 2008. Her master's thesis was on the analysis of creeping flow of particles in microconduits. She received her B.S. in mechanical engineering in 2006 from Jadavpur University, India. Her doctoral research is focused on thermal management for engineering systems and electronic devices using graphene and ultrathin graphite.

Rodney S. Ruoff holds the Cockrell Family Regents Chair at the University of Texas at Austin, after having been director of the Biologically Inspired Materials Institute at Northwestern University. He received his B.S. in chemistry from University of Texas at Austin and Ph.D. in chemical physics from the University of Illinois–Urbana (advisor H. S. Gutowsky). Prior to Northwestern University he was a staff scientist at the Molecular Physics Laboratory, SRI International, and then an associate professor of physics at Washington University. He is a cofounder of Graphene Energy, Inc., founder of Graphene Materials LLC, founder of Nanode, Inc., and author of more than 200 refereed articles in materials science, physics, mechanics, chemistry, electrochemical energy storage, and biomedical research.

Andrew Fleming is a mechanical engineer in the Air Force Research Laboratory, Propulsion Directorate, Energy/Power/Thermal Division, Wright-Patterson Air Force Base, Ohio. He received his bachelor's and master's degrees from Wright State University. His research interests include acceleration effects on two-phase thermal management systems, loop heat pipes, electronics cooling as applied to aircraft applications, and advanced heat exchanger technology.